Proceedings of the XVII Vibration Engineering & Technology of Machinery Conference
VETOMAC 2022
December 15 - 17, 2022, Institute of Engineering Pulchowk, Tribhuvan University, Nepal

VETOMAC2022-XXX

DYNAMIC MODELLING AND RESPONSE OF A PELTON BUCKET

Amrit Tiwari
Research Scholar
Department of Mechanical and Aerospace Engineering
IOE, Pulchowk Campus
Email: 076msmde001.amrit@pcampus.edu.np

Mahesh Chandra Luintel, Ph.D.
Professor
Department of Mechanical and Aerospace Engineering
IOE, Pulchowk Campus
Email: mcluintel@ioe.edu.np Email:

Sandip Ghimire
Research Scholar
Department of Mechanical and Aerospace Engineering
IOE, Pulchowk Campus
Email: 076msmde016.sandip@pcampus.edu.np

Bir Bahadur Chaudhary
Research Scholar
Department of Mechanical and Aerospace Engineering
IOE, Pulchowk Campus
Email: 076msmde004.bir@pcampus.edu.np

ABSTRACT

The study of rotating cantilever beam has a wide range of practical engineering applications, including turbine blades, aircraft wings, etc. From the literature review, it was perceived that the research works lack the use of a rotating cantilever beam model for the vibrational study of a bucket of the Pelton turbine. This research work focuses the study of vibrational characteristics of a single bucket in the Pelton turbine under the action of jet force considering it as a rotating cantilever beam. The potential and kinetic energy are determined to obtain the mathematical model. Hamilton's principle is used to construct the governing equations for Cartesian deformation variables which include axial, and transverse deformations. Coriolis and Centrifugal Effects are indulged automatically, rather than the aid of ad hoc provisions. The dynamic force imparted by water jet is modeled in harmonic series by using Fourier Expansion. Equations were discretized using Galerkin's Method to obtain the dynamic response of the system. Performing the analysis in the bucket of length $75mm$ *and attached with rotor rotating at speed of 1500 rpm, the first lower natural frequency is found to be* $5281.4\ Hz$ *in the direction of jet for the first mode of vibration and the effect of Coriolis terms in natural frequency is found to be insignificant due to shorter length of the bucket. The bending stiffness was found to be increased with the increase in the rotational speed. Forced vibration analysis is carried out to determine the steady-state amplitudes of bending vibration. In the direction of jet, the maximum deformation is found to be* $1.921\ \mu m$*. The findings can be used as a guide for the dynamic analysis as well as a basis for design or advancement.*

Keywords: ***Rotating Cantilever beam, Pelton bucket, forced vibration, Hamilton principle, rotor dynamics***

NOMENCLATURE

I_y	Moment of inertia along y-axis
I_z	Moment of inertia along z-axis
W_{nc}	Work done by external force
δ_d	Dirac delta function
ϕ_i	Assumed mode function in longitudinal direction
ψ_i	Assumed mode function in transverse direction
A	Cross Section area of bucket
E	Modulus of elasticity
i, j, k	Unit vectors along x, y and z axis respectively
L	Length of the bucket
nm	Nanometer
T	Kinetic Energy of the system
U	Strain Energy of the system
F_j	Jet force exerted to a bucket
a	Distance between point of rotation and fixed end
$u(x,t)$	Deformation along x-axis
$v(x,t)$	Deformation along y-axis
$w(x,t)$	Deformation along z-axis
x	Longitudinal axis direction of bucket
y	Jet force direction
z	Direction perpendicular to jet force
μm	Micrometer
ρ	Density of bucket materials
ω	Frequency of jet force in the bucket (rad/s)
Ω	Rotational speed of runner (rad/s)

1. INTRODUCTION

As just a large machine used in several hydropower plants, the hydro turbine, of which operation is crucial to the country's economy, is always high priority for those working in the field [1]. A Pelton turbine, sometimes known as a Pelton wheel, is a form of hydro turbine (more specifically, an impulse turbine) that is commonly seen in hydroelectric plants. On the disc, buckets are mounted. When the jet hits with the buckets, the bucket rotates. The jet forces set the bucket to vibration under different excitation modes. For the better mastery of machine's operations and failures, it is essential to look into the system's dynamic characteristics. The dynamic analysis of Pelton bucket can be carried out by considering it a rotating cantilever beam. Numerous real-world engineering applications, including turbine blades and aircraft rotary wings, utilize rotating cantilever beams [2]. Rotating beam have some deviation from non-rotating beams because of centrifugal and Coriolis effects on its dynamics.

Material fatigue, unrecognized vibration in the buckets, and crack in the root area, in which the material stress is caused by the periodic deformation, are among the most serious issues with Pelton turbine operation [3].Several vibrational study works has been carried out so far in the Pelton turbine unit. Rajak et al. [4] used Lagrange equations followed by the Rayleigh-Ritz method to perform a dynamic analysis of the Pelton turbine and assembly in order to determine the system's natural frequency. Karki et al. [5] conducted research to model the excitation force that is imparted by a jet in the form of a harmonic series and studied the forced response analytically of a simply supported Pelton turbine unit. The experimental result was compared to the analytically determined amplitude of forced vibration, and the influence of shaft rotational speed on the amplitude of vibration was evaluated. Similarly, Tharu et al. [6] focused on the dynamics of Pelton turbine unit with flexible rotor bearings at the support ends. They performed free and forced vibration analysis and the analytical results of systems with flexible and rigid bearings were also compared.

In the study of the dynamics of a cantilever beam attached to a rotating rigid body, Kane and Ryan [7] took into account effects like centrifugal stiffening and vibration driven on by Coriolis forces. On the premise of this reference, Yoo et al. [8] established an accurate linear modelling approach for flexible beams that are encountering high overall motion and accompanying low linear elastic deformations. Similar work was done by Yoo and Shin [2] who conducted a vibrational study of a rotating cantilever beam and contrast it with a nonrotating beam. It was found that the vibration properties of rotating beams varied greatly from those of non-rotating beams. The variation is brought on by strain produced on by the rotation's centrifugal inertia force. Kaya [9] had seen the growing interest in the study of the vibration characteristics of rotating elastic structures. He had used the Rayleigh energy theorem to create straightforward equation that calculates resonance frequency of a rotating beam structures. Luintel and Vyas [10] conducted study on the stability and response of a spinning turbine blade to pitching and yawing motions. A cantilever blade with a uniform cross section area that is mounted on a revolving disk is used to represent a turbine blade in models. Partial Differential equation was converted into time domain ordinary differential equation by using Galerkin method. A rotating tapered and twisted Rayleigh beam was subjected to a modal analysis by Hoskoti et al. [11] using a Langragian approach. They varied several parameters, such as taper ratio, pretwisted angle and rotating speed to observe the impact on modal frequency. The beam was modelled as rotating cantilever beam and stretch bending-torsion motion were coupled.

2. MATHEMATICAL MODEL DEVELOPMENT

2.1 System Description

Consider a cantilever bucket, modeled as cantilever beam, having length L which is fixed with the rigid runner as shown in Fig. 1 . The deformation is represented by three Cartesian Variables. The variables $u(x,t)$ denotes deformation along axial direction while $v(x,t)$ and $w(x,t)$ represent the same in direction of jet(Flap wise) and direction in perpendicular to jet (Chord wise) respectively. The bucket is characterized by material properties; Elasticity E and density ρ, cross sectional properties area $A(x)$, Moment of inertia $I_y(x)$and $I_z(x)$. L is the length of bucket from point O and a is the distance from point of rotation and point O.

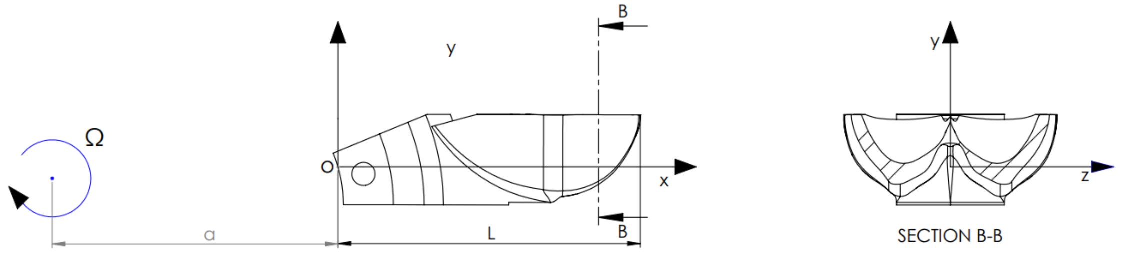

Fig. 1 Rotating Bucket subjected to jet force

For this research study, the mentioned assumptions were made:

- The bucket is assumed to be homogeneous and have isotropic material properties.
- The beam is modelled as Euler Bernoulli Beam where the Shear effect and the rotary effect is neglected.
- The runner is assumed to be rigid and is rotating about axis of symmetry with a constant rotating speed of Ω.
- The jet force is considered as a point force acting at the distance of 2L/3 from the fixed end.

2.2 Kinetic Energy

The velocity at point as the combination of movement of an arbitrary point and a rotational effect about point O can be written as:

$$\mathbf{V}=\begin{bmatrix}\dot{u}\\ \dot{v}\\ \dot{w}\end{bmatrix}+\begin{bmatrix}0\\ 0\\ \Omega\end{bmatrix}\times\begin{bmatrix}a+x+u\\ v\\ w\end{bmatrix}=(\dot{u}-\Omega v)\hat{\imath}+\big(\dot{v}+\Omega(a+x+u)\big)\hat{\jmath}+\dot{w}\hat{k} \tag{1}$$

$$\begin{aligned}T&=\frac{1}{2}\int_0^L \rho A(x)\,\boldsymbol{V}.\mathbf{V}dx=\frac{1}{2}\int_0^L \rho A(x)\,\{[\dot{u}-\Omega v]^2+[\dot{v}+\Omega(a+x+u)]^2+\dot{w}^2\}dx\\ &=\frac{1}{2}\int_0^L \rho A(x)\,\rho A(x)\,[\dot{u}^2+\Omega^2v^2-2\Omega v\dot{u}+\dot{v}^2+\Omega^2(a+x+u)^2+2\Omega\dot{v}(a+x+u)\\ &\quad+\dot{w}^2]dx\end{aligned} \tag{2}$$

2.3 Potential Energy

The axial normal strain in the x direction can be represented as follows using the von Karman theory,

$$\begin{aligned}\varepsilon_x&=u'+\frac{1}{2}(v')^2+\frac{1}{2}(w')^2-yv''-zw''\\ \sigma&=E\varepsilon_x=E\left(u'+\frac{1}{2}(v')^2+\frac{1}{2}(w')^2-yv''-zw''\right)\end{aligned} \tag{3}$$

The strain energy or potential energy of the beam can be written as.

$$\begin{aligned}U&=\frac{1}{2}\int_V \sigma\varepsilon_x\,dV=\frac{1}{2}E\int_0^L\int_A\left(u'+\frac{1}{2}(v')^2+\frac{1}{2}(w')^2-yv''-zw'\right)^2 dAdx\\ &=\frac{1}{2}E\int_0^L\int_A (u')^2\,dAdx+\frac{1}{8}E\int_0^L\int_A (v')^4\,dAdx+\frac{1}{8}E\int_0^L\int_A (w')^4\,dAdx\\ &+\frac{1}{4}E\int_0^L\int_A (v')^2(w')^2\,dAdx+\frac{1}{2}E\int_0^L\int_A u'(v')^2\,dAdx+\frac{1}{2}E\int_0^L\int_A u'(w')^2\,dAdx\\ &+\frac{1}{2}E\int_0^L\int_A y^2(v'')^2\,dAdx+\frac{1}{2}E\int_0^L\int_A z^2(w'')^2\,dAdx\\ &=\frac{1}{2}E\int_0^L A(x)(u')^2dx+\frac{1}{8}E\int_0^L A(x)(v')^4dx+\frac{1}{8}E\int_0^L A(x)(w')^4dx\\ &+\frac{1}{4}E\int_0^L A(x)(v')^2(w')^2dx+\frac{1}{2}E\int_0^L A(x)\,u'(v')^2dx\\ &+\frac{1}{2}E\int_0^L A(x)\,u'(w')^2dx+\frac{1}{2}E\int_0^L I_z(x)\,(v'')^2dx+\frac{1}{2}E\int_0^L I_y(x)(w'')^2dx\end{aligned} \tag{4}$$

2.4 Work Done

The work is done by the impact force which is assumed to be acted on the distance of $2L/3$ along the center line.

$$\delta W_{nc}=\int_0^L F(t)\delta_d\left(x-\frac{2L}{3}\right)\,\delta v\,dx \tag{5}$$

$$\delta_d \text{ is a dirac delta function with } \delta_d=1 \text{ when } x=\frac{2L}{3} \text{ and } \delta_d=0 \text{ when } x\neq\frac{2L}{3}$$

Applying the Hamilton's Principle, $\delta\int_{t_1}^{t_2}(T-V)dt+\delta\int_{t_1}^{t_2}W_{nc}\,dt=0$, three governing equations of motion are determined:

$$\rho A(x)\,\ddot{u}-\rho A(x)\,\Omega^2 u-2\rho A(x)\,\Omega\dot{v}-E\frac{\partial}{\partial x}\left(A(x)\frac{\partial u}{\partial x}\right)-\frac{1}{2}E\frac{\partial}{\partial x}\left(A(x)\left(\frac{\partial v}{\partial x}\right)^2\right)-\frac{1}{2}E\frac{\partial}{\partial x}\left(A(x)\left(\frac{\partial w}{\partial x}\right)^2\right)=\rho A(x)\,\Omega^2(a+x) \tag{6}$$

$$\rho A(x)\,\ddot{v}-\rho A(x)\,\Omega^2 v+2\rho A(x)\Omega\dot{u}+E\frac{\partial^2}{\partial x^2}\left(I_z(x)\frac{\partial^2 v}{\partial x^2}\right)-E\frac{\partial}{\partial x}\left(A(x)\frac{\partial u}{\partial x}\frac{\partial v}{\partial x}\right)-\frac{1}{2}E\frac{\partial}{\partial x}\left(A(x)\frac{\partial v}{\partial x}\left(\frac{\partial w}{\partial x}\right)^2\right)-\frac{1}{2}E\frac{\partial}{\partial x}\left(A(x)\left(\frac{\partial v}{\partial x}\right)^3\right)=F(t)\delta_d\left(x-\frac{2L}{3}\right) \tag{7}$$

$$\rho A(x)\,\ddot{w}+E\frac{\partial^2}{\partial x^2}\left(I_y(x)\frac{\partial^2 w}{\partial x^2}\right)-E\frac{\partial}{\partial x}\left(A(x)\frac{\partial u}{\partial x}\frac{\partial w}{\partial x}\right)-\frac{1}{2}E\frac{\partial}{\partial x}\left(A(x)\left(\frac{\partial v}{\partial x}\right)^2\frac{\partial w}{\partial x}\right)-\frac{1}{2}E\frac{\partial}{\partial x}\left(A(x)\left(\frac{\partial w}{\partial x}\right)^3\right)=0 \tag{8}$$

The associated boundary conditions are:

$$u=v=w=\frac{\partial v}{\partial x}=\frac{\partial w}{\partial x}=0 \text{ at } x=0$$
$$\frac{\partial u}{\partial x}=\frac{\partial^2 v}{\partial x^2}=\frac{\partial^3 v}{\partial x^3}=\frac{\partial^2 w}{\partial x^2}=\frac{\partial^3 v}{\partial x^3}=\frac{\partial^3 w}{\partial x^3}=0 \tag{9}$$

Equation of axial deformation (Eq. 6) contains time independent steady centrifugal force terms ; $\boldsymbol{\rho A(x)\ \Omega^2(a+x)}$, so we can decompose the axial deformation into time independent steady state axial deformation $u_s(x)$, arises due to forces from rotational effect, and time dependent vibration response $u_d(x,t)$. The above three equation are now written as:

$$-\rho A(x)\,\Omega^2 u_s-E\frac{d}{dx}(A(x))\frac{du_s}{dx}-E\,A(x)\frac{d^2 u_s}{dx^2}=\rho A(x)\,\Omega^2(a+x) \tag{10}$$

$$\rho A(x)\,\ddot{u}_d-\rho A(x)\,\Omega^2 u_d-2\rho A(x)\,\Omega\dot{v}-E\frac{\partial}{\partial x}\left(A(x)\frac{\partial u_d}{\partial x}\right)-\frac{1}{2}E\frac{\partial}{\partial x}\left(A(x)\left(\frac{\partial v}{\partial x}\right)^2\right)-\frac{1}{2}E\frac{\partial}{\partial x}\left(A(x)\left(\frac{\partial w}{\partial x}\right)^2\right)=0 \tag{11}$$

$$\rho A(x)\,\ddot{v}-\rho A(x)\,\Omega^2 v+2\rho A(x)\Omega\dot{u}_d+E\frac{\partial^2}{\partial x^2}\left(I_z(x)\frac{\partial^2 v}{\partial x^2}\right)-E\frac{\partial}{\partial x}\left(A(x)\frac{du_s}{dx}\frac{\partial v}{\partial x}\right)-E\frac{\partial}{\partial x}\left(A(x)\frac{\partial u_d}{\partial x}\frac{\partial v}{\partial x}\right)-\frac{1}{2}E\frac{\partial}{\partial x}\left(A(x)\frac{\partial v}{\partial x}\left(\frac{\partial w}{\partial x}\right)^2\right)-\frac{1}{2}E\frac{\partial}{\partial x}\left(A(x)\left(\frac{\partial v}{\partial x}\right)^3\right)=F(t)\delta_d\left(x-\frac{2L}{3}\right) \tag{12}$$

$$\rho A(x)\,\ddot{w}+E\frac{\partial^2}{\partial x^2}\left(I_y(x)\frac{\partial^2 w}{\partial x^2}\right)-E\frac{\partial}{\partial x}\left(A(x)\frac{du_s}{dx}\frac{\partial w}{\partial x}\right)-E\frac{\partial}{\partial x}\left(A(x)\frac{\partial u_d}{\partial x}\frac{\partial w}{\partial x}\right)-\frac{1}{2}E\frac{\partial}{\partial x}\left(A(x)\left(\frac{\partial v}{\partial x}\right)^2\frac{\partial w}{\partial x}\right)-\frac{1}{2}E\frac{\partial}{\partial x}\left(A(x)\left(\frac{\partial w}{\partial x}\right)^3\right)=0 \tag{13}$$

2.5 Discretization of the Equations of Motion

The partial differential system of equation is converted into ordinary system of differential equation by using Galerkin Method. The deformations are assumed to be in the form:

$$u_s(x)=\sum \Psi_i(x)A_i=\Psi_s^T(x)A_s \tag{14}$$
$$u_d(t,x)=\sum \Psi_i(x)U_i(t) \tag{15}$$
$$v(t,x)=\sum \phi_i(x)V_i(t) \tag{16}$$
$$w(t,x)=\sum \phi_i(x)W(t) \tag{17}$$

The assumed mode function taken for the axial direction and transverse direction of the beam are:

$$\Psi_i=\sqrt{2}\sin\left(\frac{2i-1}{2L}\pi x\right)\qquad i=1,2,3,\ldots. \tag{18}$$

$$\phi_i=\cosh(\beta_i x)-\cos(\beta_i x)-\frac{\cosh\beta_i+\cos\beta_i}{\sinh\beta_i+\sin\beta_i}\left(\sinh(\beta_i x)-\sin(\beta_i x)\right) \tag{19}$$
$$\text{where, } \beta_i L=1.875, 4.694, 7.855, 10.995, \ldots.. \quad \text{for } i=1,2,3,4\ldots.\text{respectively}$$

2.6 Static Axial Deformation

Using Galerkin method

$$\int_0^L \Psi_s(x)\, R\ \ dx = 0 \tag{20}$$

The linear matrix equation can be obtained in the form

$$K_s A_s = F_s \tag{21}$$

Where,

$$K_s = \int_0^L \left(\rho A(x)\Omega^2 \Psi_s \Psi_s^T + E\frac{d}{dx}\big(A(x)\big)\Psi_s \frac{d\Psi_s^T}{dx} + EA(x)\Psi_s \frac{d^2\Psi_s^T}{dx^2}\right) dx \qquad F_s = -\int_0^L \rho A(x)\ \ \Omega^2 (a+x)\Psi_s\, dx$$

2.7 Dynamic Deformation in Axial and Transverse Direction

On applying the Galerkin method with single assumed mode (i^{th} mode as: Ψ_i and ϕ_i) for axial and transverse direction. The nonlinear coupled equation is obtained as given:

$$M_{11}\ddot{U} + C_{12}\dot{V} + K_{11}U + K_{q12}V^2 + K_{q13}W^2 = 0 \tag{22}$$

$$M_{22}\ddot{V} + C_{21}\dot{U} + K_{22}V + K_{q21}VU + K_{c22w}W^2V + K_{c22v}V^3 = f_2 \tag{23}$$

$$M_{33}\ddot{W} + K_{33}W + K_{q31}WU + K_{c33v}V^2W + K_{c33w}W^3 = 0 \tag{24}$$

Where,

$$M_{11} = \int_0^L \rho A(x)\ \ \Psi_i^{\,2}\ \ dx \qquad M_{22} = \int_0^L \rho A(x)\ \phi_i^2\ dx \qquad M_{33} = \int_0^L \rho A(x)\ \phi_i^2\ dx$$

$$C_{12} = -\int_0^L 2\rho A(x)\ \ \Omega\, \Psi_i\ \phi_i\ dx \qquad C_{21} = \int_0^L 2\rho A(x)\ \ \Omega\, \Psi_i\ \phi_i\ dx$$

$$K_{11} = \int_0^L \left[-\rho A(x)\ \ \Omega^2\ \ \Psi_i^2 - \ E\,\Psi_i\ \frac{d\Psi_i}{dx}\frac{d}{dx}\big(\ A(x)\big)\ - E\ A(x)\ \Psi_i \left(\frac{d^2\Psi_i}{dx^2}\right)\right] dx$$

$$K_{22} = \int_0^L \Bigg[-\ \rho A(x)\ \Omega^2\phi_i^2 +\ E\ I_z(x)\phi_i\ \frac{d^4\phi_i}{dx^4}\ + 2E\frac{d}{dx}\big(\ I_z(x)\big)\phi_i\ \frac{d^3\phi_i}{dx^3} +\ E\frac{d^2}{dx^2}\big(I_z(x)\big)\ \phi_i\ \frac{d^2\phi_i}{dx^2}$$
$$-\ E\,A(x)\ \ \frac{d^2u_s}{dx^2}\phi_i\ \frac{d\Psi_i}{dx} - E\,A(x)\ \frac{du_s}{dx}\ \phi_i\ \frac{d^2\Psi_i}{dx^2} - E\frac{d}{dx}\big(\ A(x)\big)\frac{du_s}{dx}\ \phi_i\frac{d\Psi_i}{dx}\Bigg] dx$$

$$K_{33} = \int_0^L \Bigg[\ E\ I_y(x)\phi_i\ \frac{d^4\phi_i}{dx^4}\ + 2E\frac{d}{dx}\big(I_y(x)\big)\phi_i\ \frac{d^3\phi^T}{dx^3} + E\ \frac{d^2}{dx^2}\big(\ I_y(x)\big)\ \phi_i\ \frac{d^2\phi_i}{dx^2}\ -\ E\ A(x)\ \ \frac{d^2u_s}{dx^2}\phi_i\ \frac{d\Psi_i}{dx}$$
$$-\ E\ A(x)\ \frac{du_s}{dx}\phi_i\ \frac{d^2\Psi_i}{dx^2} - E\frac{d}{dx}\big(A(x)\big)\ \frac{du_s}{dx}\phi_i\frac{d\Psi_i}{dx}\Bigg] dx$$

$$K_{q12} = \int_0^L \left[-\frac{1}{2}E\frac{d}{dx}\big(\ A(x)\big)\ \Psi_i\ \ \left(\frac{d\phi_i}{dx}\right)^2\ - E\ A(x)\ \ \Psi_i\ \ \frac{d\phi_i}{dx}\ \frac{d^2\phi_i}{dx^2}\right] dx$$

$$K_{q13} = \int_0^L \left[-\frac{1}{2}E\frac{d}{dx}\big(A(x)\big)\ \Psi_i\ \left(\frac{d\phi_i}{dx}\right)^2\ - E\ A(x)\ \Psi_i\ \ \frac{d\phi_i}{dx}\ \frac{d^2\phi_i}{dx^2}\right] dx$$

$$K_{q21} = \int_0^L \left[-\ E\ A(x)\ \phi_i\ \ \frac{d^2\phi_i}{dx^2}\ \frac{d\Psi_i}{dx}\ - E\ A(x)\ \phi_i\ \ \frac{d\phi_i}{dx}\ \ \frac{d^2\Psi_i}{dx^2} - E\frac{d}{dx}\big(A(x)\big)\phi_i\ \frac{d\phi_i}{dx}\frac{d\Psi_i}{dx}\right] dx$$

$$K_{q31} = \int_0^L \left[-\ E\ A(x)\ \phi_i\ \ \frac{d^2\phi_i}{dx^2}\ \frac{d\Psi_i}{dx}\ - E\ A(x)\ \phi_i\ \ \frac{d\phi_i}{dx}\ \ \frac{d^2\Psi_i}{dx^2} - E\frac{d}{dx}\big(A(x)\big)\phi_i\ \frac{d\phi_i}{dx}\frac{d\Psi_i}{dx}\right] dx$$

$$K_{c22w} = \int_0^L \left[-E\ A(x)\phi\ \frac{d^2\phi_i}{dx^2}\frac{d\phi_i}{dx}\frac{d\phi_i}{dx} - \frac{1}{2}E\ A(x)\phi_i\left(\frac{d\phi_i}{dx}\right)^2\frac{d^2\phi_i}{dx^2} - \frac{1}{2}E\frac{d}{dx}\big(A(x)\big)\phi_i\ \left(\frac{d\phi_i}{dx}\right)^3\right] dx$$

$$K_{c22v} = \int_0^L \left[\ -\frac{1}{2}E\frac{d}{dx}\big(\ A(x)\big)\ \phi_i\ \ \left(\frac{d\phi_i}{dx}\right)^3\ -\frac{3}{2}\ E\ A(x)\ \phi_i\ \ \left(\frac{d\phi_i}{dx}\right)^2\ \frac{d^2\phi_i}{dx^2}\right] dx$$

$$K_{c33v} = \int_0^L \left[-E\ A(x)\phi_i\ \ \frac{d^2\phi}{dx^2}\left(\frac{d\phi_i}{dx}\right)^2 - \frac{1}{2}E\ A(x)\ \phi_i\ \left(\frac{d\phi_i}{dx}\right)^2\frac{d^2\phi_i}{dx^2} - \frac{1}{2}E\frac{d}{dx}\big(\ A(x)\big)\ \phi_i\ \ \left(\frac{d\phi_i}{dx}\right)^3\ \right] dx$$

$$K_{c33w} = \int_0^L \left[\ -\frac{1}{2}E\frac{d}{dx}\big(\ A(x)\big)\phi_i\ \ \left(\frac{d\phi_i}{dx}\right)^3\ -\frac{3}{2}\ E\ A(x)\ \phi_i\ \ \left(\frac{d\phi_i}{dx}\right)^2\ \frac{d^2\phi_i}{dx^2}\right] dx$$

2.8 Representation of Force Exerted by Jet in Harmonic Series

For a Pelton bucket, after the each complete rotation of the wheel, the bucket will get the impact. So periodic impact is obtained in the bucket. The forcing term will appear to be a series of separate events rather than a continuous function .These forces can be modelled using impulses as shown in Fig. 2 .

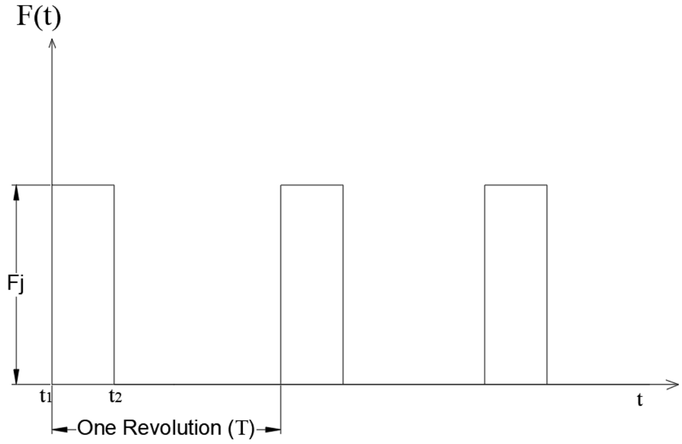

Fig. 2 Force Exerted by jet on a bucket

The force due to water jet can be defined for a period T mathematically as

$$F(t) = \begin{Bmatrix} F_j \text{ for } t_1 \leq t \leq t_2 \\ 0 \text{ for } t_2 < t < t_3 \end{Bmatrix} \tag{25}$$

For the vibration analysis, this periodic force need to be modeled as a series of harmonic forces. Fourier series expansion is used to convert the non-harmonic periodic force into harmonic terms and the expression is given as [12]

$$F(t) = \frac{a_0}{2} + \sum_{n=1}^{\infty} (a_n \cos n\omega t + b_n \sin n\omega t) \tag{26}$$

Where,

$$a_0 = \frac{2}{T}\int_0^T F(t)dt \;,\; a_n = \frac{2}{T}\int_0^T F(t)\cos n\omega t\, dt \;,\; b_n = \frac{2}{T}\int_0^T F(t)\sin n\omega t\, dt$$

The calculation of jet force for the Pelton turbine unit is taken from Karki et. al. [5].

2.9 Specification of Pelton Bucket

Following parameters will be used for the study:

Table 1 Specification of Pelton Bucket

Force exerted by jet to buckets	193 N [5]
Rated rpm of Turbine	1500 rpm
Diameter of runner (tip to tip)	204 mm
Pitch circle Diameter of runner (PCD)	155 mm
No of Buckets	16
Gap Between consecutive buckets	12.434 mm
Length of bucket from base area	75 mm
Distance of base plane from center of rotation	0.1m
Modulus of Elasticity of bucket materials(Casted Brass)	110 Gpa
Density of bucket materials (Casted Brass)	8520 kg/m^3

The bucket under study, though having its own shape, it is assumed to be of a beam with the length of 75mm with the cross section properties that varies along the length as given by Eq. 27, Eq. 28 and Eq. 29. The cross-section properties are determined by using CAD model of bucket. The section properties in each planes are observed and the values of Area, Moment of inertia along z axis and that along y axis are obtained. The data obtained are used to fit the best curve (Polynomial Expression) that gives the cross sectional properties in each plane at a distance of x from base plane. This model of beam will be used for the mathematical solution.

$$A(x) = 0.0003613871 - 0.03286114x + 4.099293x^2 - 136.2764x^3 + 1776.146x^4 - 8242.621x^5 \ m^2 \quad (27)$$

$$I_z(x) = 0.8030534 * 10^{-8} - 0.1909915 * 10^{-5}x + 0.0002580086x^2 - 0.008972585x^3 + 0.1212268x^4 - 0.5756649x^5 \ m^4 \quad (28)$$

$$I_y(x) = 0.1828805 * 10^{-7} - 0.4528189 * 10^{-5}x + 0.0004345548x^2 - 0.01108898x^3 + 0.1285104x^4 - 0.6340727x^5 \ m^4 \quad (29)$$

3. RESULTS

3.1 Static Deformation

The static deformation is calculated for the different number of modes taken into consideration and the calculation of A_s gives the static deformation solution. On checking the convergence of the solution, it was found that the solution converges well when three or more numbers of modes are taken into consideration which is represented by Fig. 3 below.

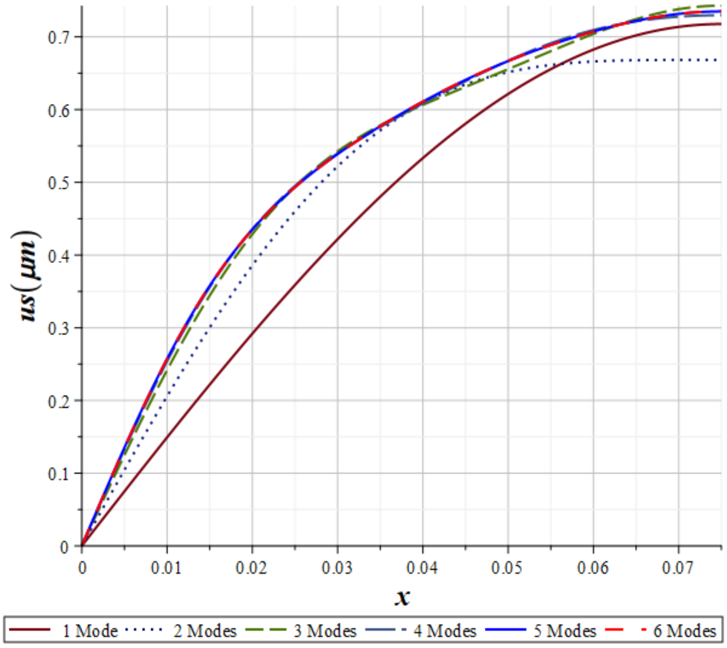

Fig. 3 Static response in the axial direction for different numbers of modes.

The solution of static deformation as a spatial function with six modes in consideration is obtained as:

$$u_s = 5.62 * 10^{-7} * \sqrt{2}\sin\left(\frac{20}{3}\pi x\right) + 6.13 * 10^{-8} * \sqrt{2}\sin(20\pi x) + 2.39 * 10^{-8} * \sqrt{2}\sin\left(\frac{100}{3}\pi x\right) + 6.55 * 10^{-9} * \sqrt{2}\sin\left(\frac{140}{3}\pi x\right) + 1.99 * 10^{-9} * \sqrt{2}\sin(60\pi x) - 5.34 * 10^{-11} * \sqrt{2}\sin\left(\frac{220}{3}\pi x\right) \quad (30)$$

The static deformation at end of bucket $(x = L)$ is calculated to be 0.73 μm for the rotational speed of 1500 rpm.

3.2 Free Vibration Response

The coefficient in the mass matrix, damping matrix and stiffness matrix, explained in the previous chapter, are determined by using respective integral equations. The calculation is simplified by using Maple software. The particular bucket parameters, mentioned in Table 1 are used to determine these coefficients. The coefficients are determined using different assumed mode function. The coefficient from mass matrix, damping matrix and linear stiffness matrix are used for the analytical solution whereas with the inclusion of quadratic and cubic nonlinear matrix coefficient are used to solve nonlinear equation numerically.

3.2.1 Damped and Undamped Natural Frequency

Using linear coupled equation, the natural frequency in the axial, in the direction of the jet (flap wise) and perpendicular to the jet (chord wise) direction (ω_1, ω_2 , and ω_3 *respectively*) are determined using the formulas below which are derived analytically,

$$\omega_1 \text{ and } \omega_2 = \frac{1}{2\pi}\left(-\frac{1}{2M_{11}M_{22}}\Big(C_{21}C_{12} - K_{11}M_{22} - M_{11}K_{22} \pm \left(C_{12}^2C_{21}^2 - 2C_{12}C_{21}K_{11}M_{22} - 2C_{12}C_{21}K_{22}M_{11} + K_{11}^2M_{22}^2 - 2M_{11}M_{22}K_{11}K_{22} + K_{22}^2M_{11}^2\right)^{\frac{1}{2}}\Big)\right)^{\frac{1}{2}} \tag{31}$$

$$\omega_3 = \frac{1}{2\pi}\sqrt{\left(\frac{K_{33}}{M_{33}}\right)} \tag{32}$$

Table 2 Natural frequency for different modes of vibration

	Axial Direction		Direction of Jet (Flap wise Direction)		Direction in perpendicular to jet (Chord wise Direction)	
	ω_1 (Hz)		ω_2 (Hz)		ω_3 (Hz)	
	Without Damping	With Damping	Without Damping	With Damping	Without Damping	With Damping
Mode 1	12974.39	12974.4	5281.47	5281.42	14740.6	14740.6
Mode 2	35073.5	35131.02	13167.7	13146.13	29104.6	29104.6
Mode 3	61217.68	61217.7	35815	35813.39	77662.6	77662.6
Mode 4	85186.2	85186.2	70374.3	70374.3	148921	148921

The comparison between damped and undammed frequency from Table 2 shows that there is negligible effect of the Coriolis term (damping) in the particular case of bucket rotating with rotational speed of 1500 rpm.

3.2.2 Variation of Natural Frequency with Rotational Speed

The rotation of the bucket will influence the centrifugal force. This centrifugal force affects the stiffness and hence the natural frequency of the bucket. The change in the natural frequency due to speed of rotation neglecting the Coriolis Effect was observed by recalculating the static deformation (u_s), and the Stiffness coefficients (K_{11}, K_{22}, K_{33}) in terms of N, where N rpm is considered to be the rotational speed of the bucket.

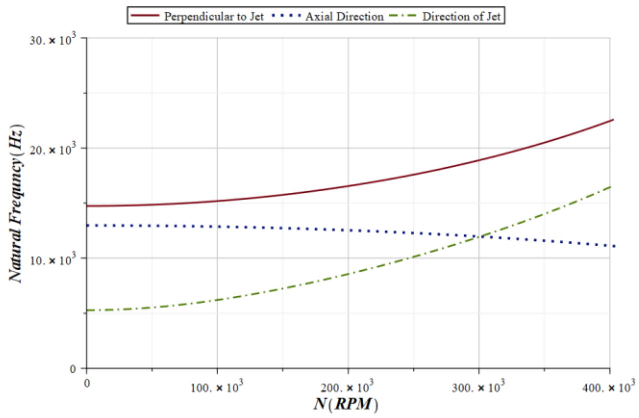

Fig. 4 Variation of First Mode Natural Frequency with Rotational Speed

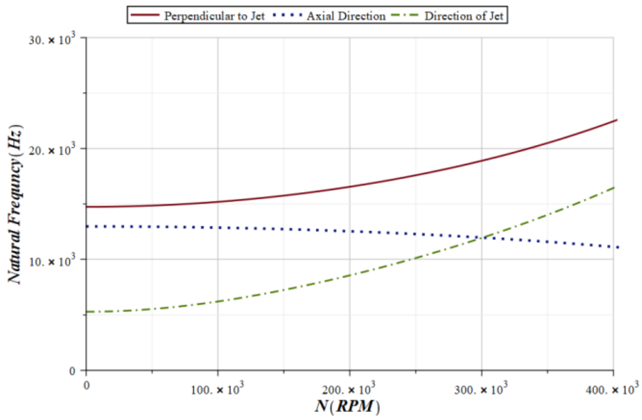

Fig. 5 Variation of Second Mode Natural Frequency with Rotational Speed

It was observed that, with the increase in the rotational speed, the stiffness and hence the natural frequency in the direction of jet and perpendicular to jet (Bending Stiffness) get increased as shown in Fig. 4 and Fig. 5 . This is due to the static stress field that is developed along the axial direction due to centrifugal force. This effect is also called as stress-stiffening. While in axial direction the stiffness and hence the natural frequency decreases with the increase in the rotational speed. This is due to the effect called as centrifugal softening. Due to the shorter length of the bucket, the effect of static centrifugal forces in stiffness in both direction are found to be small. The arguments mentioned above for natural frequency may differ while we consider the Coriolis Effect in the equations.

3.3 Validation of Mathematical Model

The natural frequency in the direction perpendicular to the jet obtained from the present study, with some formulation in the parameters, are compared with those in the works of literature for the validation of the present mathematical model. The beam is considered to be uniform with square cross section from root to tip of the bucket and given be base area value: $A = A_0 = 361.36 * 10^{-6}\ \mathrm{m}^2$ and the other geometric properties are used considering $\alpha = \sqrt{\frac{AL^2}{I}} = 70$,which were used in the study by Chung and Yoo (2002) and Zhou et. al. (2021).The value of length and moment of inertia are taken as:

$$I = I_z = I_y = 1.088336 * 10^{-8}\ \mathrm{m}^4 \quad \text{and } L = 70\sqrt{\frac{I}{A}} = 0.38416\ \mathrm{m}$$

With $a = 0$, the natural frequency for different value of rotational speed in the present model is obtained and compared as:

Table 3 Comparison of the present model with the previous study

Ω^*	Ω' rad/s	Present Study				Chung and Yoo [13]		Zhou. et.al [14]	
		Natural Frequency ω (rad/s)		Dimensionless Natural Frequency ω^*		ω^*		ω^*	
		1st Mode	2nd Mode	1st Mode	2nd Mode	1st Mode	2nd Mode	1st Mode	2nd Mode
0	0	469.8	2944.3	3.516	22.034	3.516	22.035	3.516	22.035
1	133.6	491.7	2958.9	3.680	22.143	3.681	22.181	3.682	22.181
2	267.2	552.3	3002.21	4.133	22.467	4.137	22.615	4.137	22.615
3	400.	640.7	3073.1	4.795	23.254	4.797	23.320	4.798	23.320
4	534.5	747.2	3169.7	5.592	24.10	5.584	24.273	5.587	24.275
5	668.1	865.2	3289.9	6.475	25.4201	6.449	25.446	6.453	25.451

3.4 Forced Vibration Response

3.4.1 Calculation for Fourier series Expansion

Using the Bucket Specification given in Table 1,

$$\omega = 50\pi\ \mathrm{rad/s}$$

$$t_1 = 0 \text{ second}$$

$$t_2 = \frac{37}{25000} \text{second}$$

$$F(t) = 7.28 + \sum_{n=1}^{\infty}\left(\frac{61.4}{n}\sin\left(\frac{37\pi n}{500}\right)\cos n\omega t + \frac{61.4}{n}\left(-1 + \cos\left(\frac{37\pi n}{500}\right)\right)\right) \tag{33}$$

The graphs are plotted for different numbers of Fourier components taken into consideration. Fig. 6 compares the graph for the function considering only one, first five, first ten and first twenty components. The graphs depicted that the function is approximating the shape of the force pulse, as the number of components is increased. If the function is to be obtained in accurate form, it is obvious that an infinite number of Fourier components must be taken into account. Since the graph shows that after the twentieth harmonics the representation approximated the force exerted on the bucket, the function with twenty order of harmonics is taken into consideration to determine the dynamic response due to forced vibration.

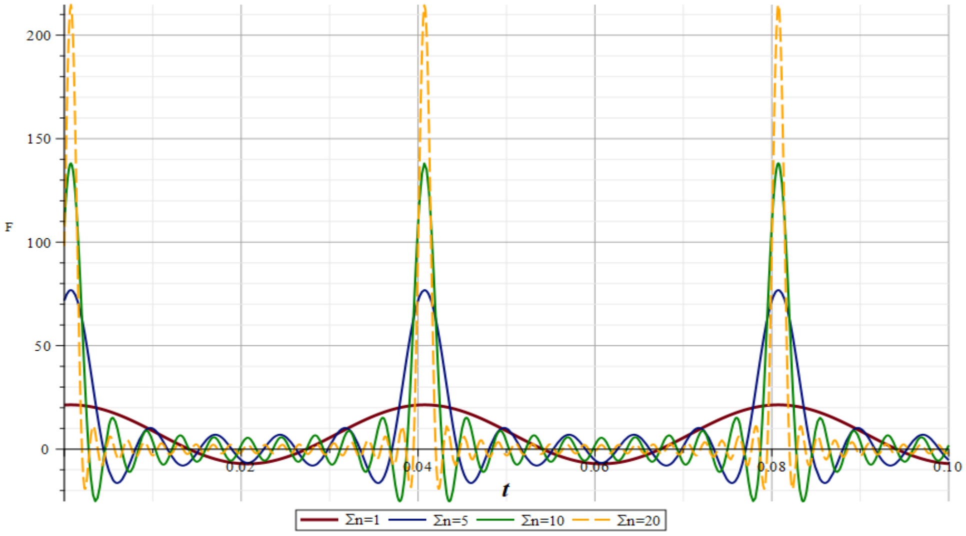

Fig. 6 Representation of Force Exerted by Jet in Harmonic Series

3.4.2 Analytical Solution for Steady State Dynamic Deformation

The steady state responses (solutions of dynamic deformation) are of the same form as the excitations acting on the system which is given by Eq. 33. For the linear dynamic equation, the motion in axial direction is coupled to the motion in the direction of jet. Hence, the steady state dynamic deformation for the solution considering the first assumed mode is written as:

$$U_1(t) = A_0 + \sum_{\substack{i=1 \\ (odd)}}^{39} A_i \, sin(iwt) + \sum_{\substack{i=2 \\ (even)}}^{40} A_i \, cos(iwt) \tag{34}$$

$$V_1(t) = B_0 + \sum_{\substack{i=1 \\ (odd)}}^{39} B_i \, sin(iwt) + \sum_{\substack{i=2 \\ (even)}}^{40} B_i \, cos(iwt) \tag{35}$$

The solution of dynamic deformation is shown in Fig. 7 and Fig. 8 . The maximum deformation in the direction of the jet is found to be 1.254 μm in the point of force applied of the bucket and 1.921 μm at the end of the bucket. Similarly, dynamic deformation is observed in the axial direction due to the Coriolis Effect. The maximum dynamic deformation in the axial direction at the end of the bucket is found to be 0.074 nm; which is very less in comparison to the static deformation, caused by centrifugal force, in the same direction.

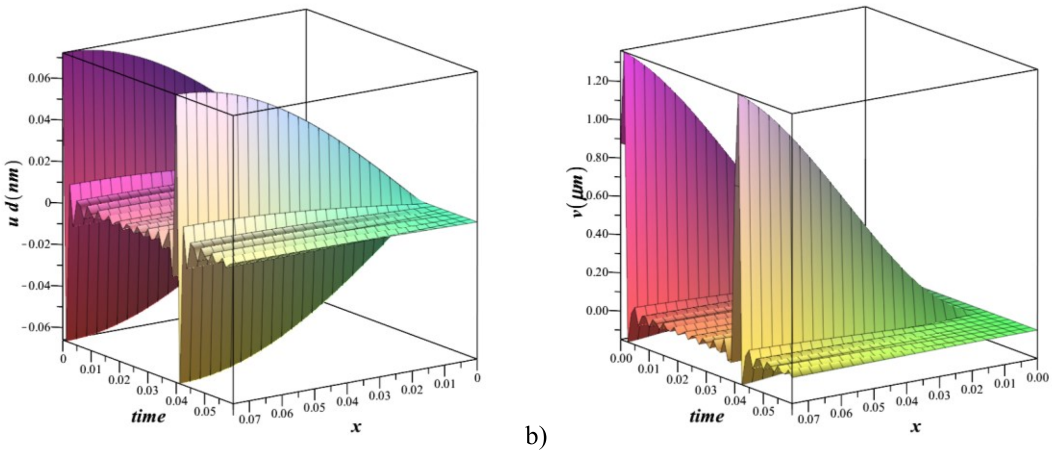

a) b)

Fig. 7 Analytical Solution for Steady State Dynamic Deformation: (a) Axial Direction, (b) Direction of jet

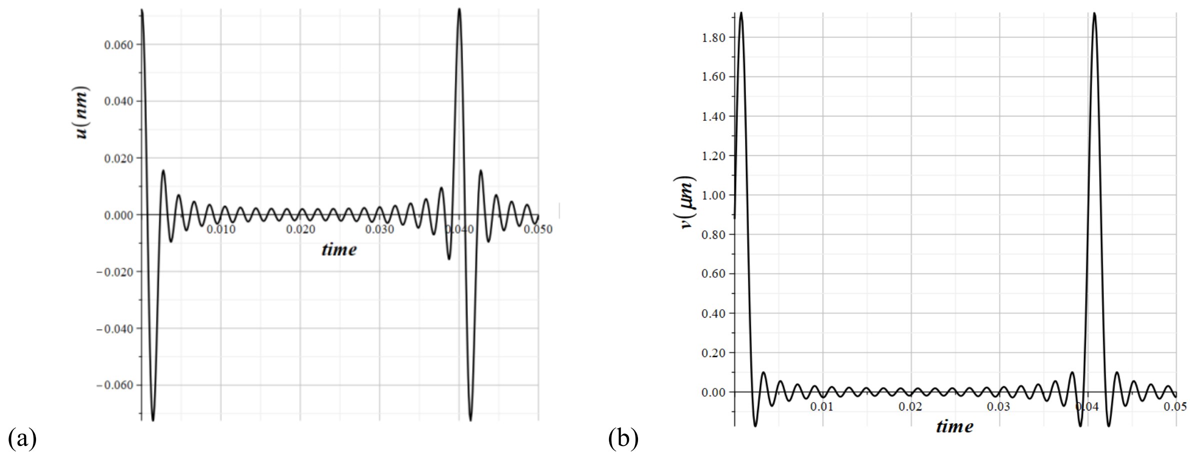

Fig. 8 Analytical dynamic response of the system at the end of Bucket: (a) Axial Direction, (b) Direction of jet

The solution is found to be converged while taking a higher number of terms from the series solution as shown in Fig. 9 . When one, two, three, and four terms are taken into consideration, the maximum displacement in the direction of the jet at the end of bucket is found to be 1.921 μm, 1.816 μm, 1.833 μm, and 1.831 μm respectively.

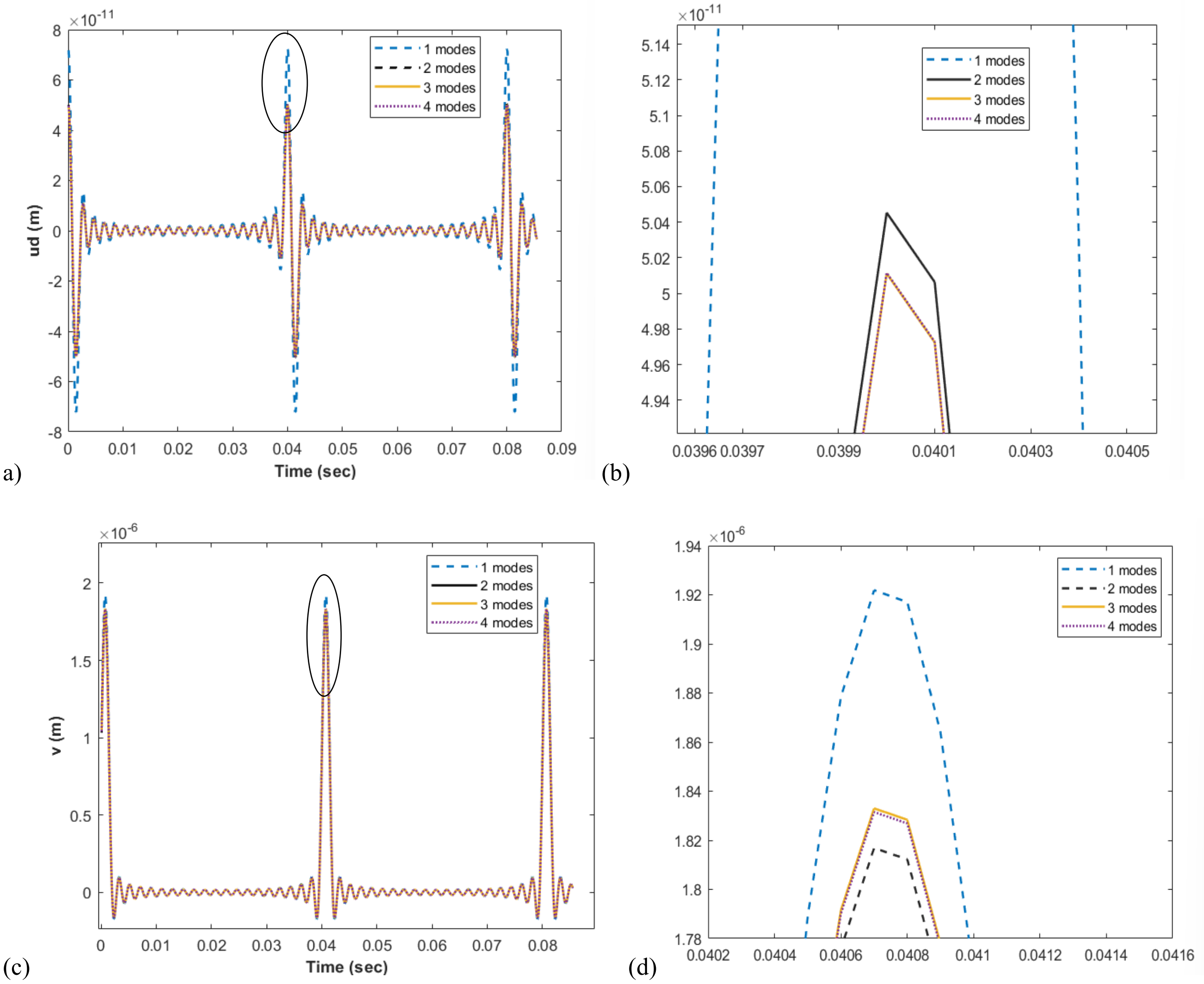

Fig. 9 Convergence of Analytical Solution at the end of bucket: (a) Axial deformation ,(b) Enlarged view showing the convergence in axial direction, (c) Direction of jet, (d) Enlarged view showing the convergence in direction of jet

3.5 Numerical Solution

For the support of the analytical solution of natural frequency, free vibration response for the first mode is also determined by using MATLAB solver for the time domain equations given by Eq. 22, Eq. (23 and Eq. 24 (Neglecting the forcing term). Free responses shown in Fig. 10 was obtained by taking any arbitary initial conditions . By using FFT, frequencies are obtained from the free response as shown in Fig. 11 The results of natural frequency from the response plot is found to be almost similar to that obtained from the previous analytical method.

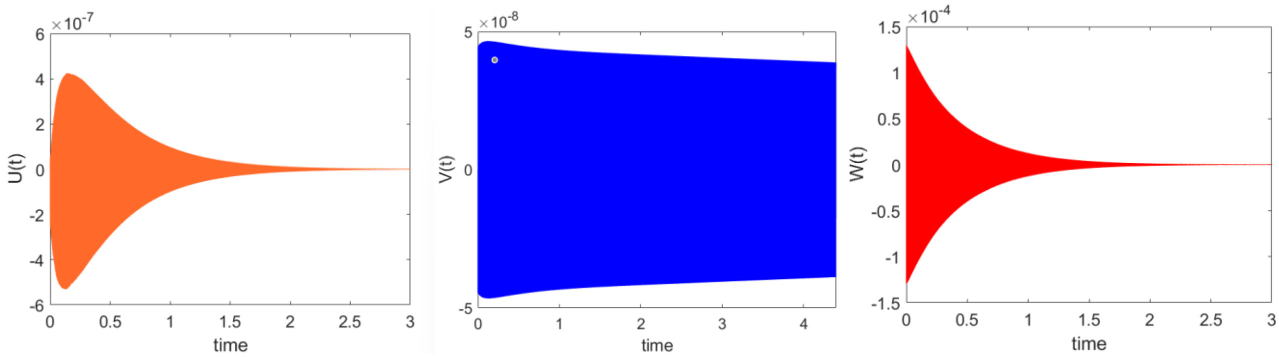

Fig. 10 Numerically obtained Free Vibration Response for first mode

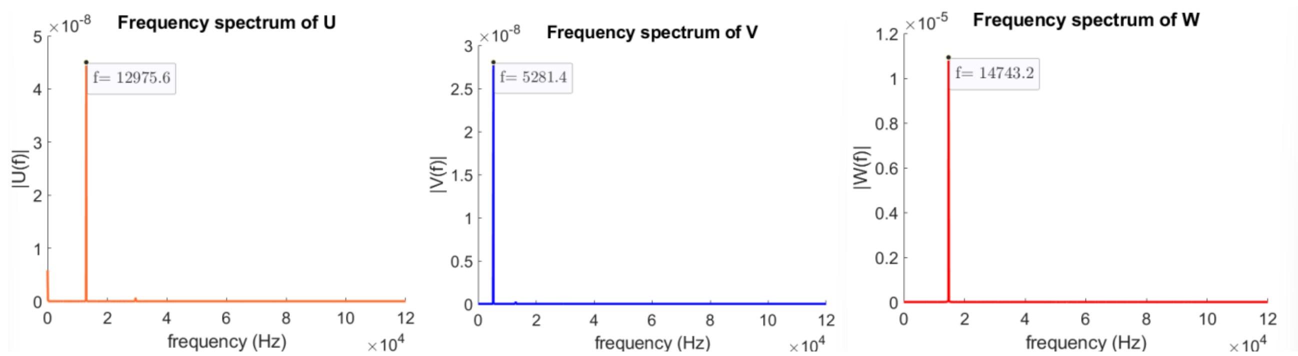

Fig. 11 Frequency Spectrum showing Natural frequency

The numerical simulation of the time domain nonlinear equation for steady response is also performed considering the first term from the series solution and all the perusal is focused on the end of the bucket. Fig. 11 shows the solution of numerical simulation. The analytical results are found to be matched fairly with the numerical results for direction of jet whereas in the axial direction, the numerical results slightly deviated from analytical one. The reason for the deviation might be the non-linearity that exists in the time domain equation which is used for numerical solution. Despite the small variation in the amplitude, the responses nature shown by both of the methods are found to be identical.

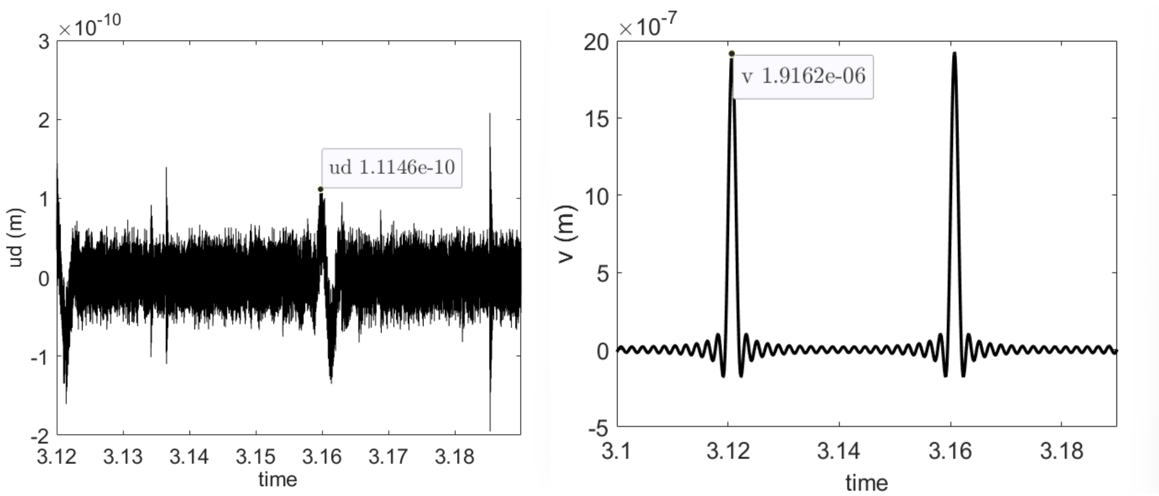

Fig. 12 Steady state responses from numerical solution: (a) Axial Direction, (b) Direction of jet

4. CONCLUSION

The conclusions drawn out from the research are as follows:

- The governing equations of the system are found to be coupled systems of the differential equation. The effects of Centrifugal and Coriolis force were observed in the equation of motion in the axial direction and the direction of the jet.
- Carrying out the study on the bucket of the test rig of Pelton turbine, rotating at the speed of 1500 rpm, the static deformation in the axial direction at the end of the bucket due to the centrifugal force was obtained 0.73 µm. The free vibration analysis showed the insignificant effects of the Coriolis terms in the natural frequency of the bucket for the speed 1500 rpm. However if the speed is made considerably high, Coriolis term do effect the natural frequency. The bending stiffness were found to be increased with increase in rotational speed whereas the axial stiffness was found to decrease.
- The force exerted by the water jet to the buckets is approximated as harmonic series up to 20th harmonic components. The jet force acting on the bucket resulted the dynamic deformation in the direction of the jet and in the axial direction too due to coupled Coriolis term in the equation of motion. However, in the axial direction, the static deformation due to centrifugal force was found to be higher than the dynamic deformation due to jet force. The amplitude was found to be maximum in the direction of the jet. In the direction of jet, the maximum amplitude was found to be 1.254 µm in the point where the force was assumed to act and 1.921 µm at the end of the bucket. The analytical solution was found to be converged well when four terms from the series solution were taken into consideration.

This research can assist in the dynamic assessment and optimization design of the bucket of the Pelton turbine in hydropower.

REFERENCES

[1] Shuren, W. (1992). Hydropower Station Building.

[2] Yoo, H. H., & Shin, S. H. (1998). Vibration analysis of rotating cantilever beams. *Journal of Sound and vibration*, 212(5), 807-828. https://doi.org/10.1006/jsvi.1997.1469.

[3] Zhang, Z. (2016): Pelton Turbines, *Springer International Publishing*, Switzerland.

[4] Rajak, A., Shrestha, P., Rijal, M., Pudasaini, B., & Luintel, M. C. (2014). Dynamic analysis of Pelton turbine and assembly. *In Proceedings of IOE Graduate Conference* (pp. 103-109).

[5] Karki, S., Luintel, M. C., & Poudel, L. (2017). Dynamic Response of Pelton Turbine Unit for Forced Vibration. In IOE Graduate Conference.

[6] Tharu, J. K., Bhatta, N., Karki, S., & Luintel, M. C. (2019). Free Vibration Analysis of Simply Supported Pelton Turbine: A Case of Flexible Rotor Bearings. In Proceedings of *IOE Graduate Conference.*

[7] Kane, T. R., Ryan, R. R., & Banerjeer, A. K. (1987). Dynamics of a cantilever beam attached to a moving base. *Journal of Guidance, Control, and Dynamics*, 10(2), 139-151. https://doi.org/10.2514/3.20195.

[8] Yoo, H. H., Ryan, R. R., & Scott, R. A. (1995). Dynamics of flexible beams undergoing overall motions. *Journal of Sound and vibration*, 181(2), 261-278. https://doi.org/10.1006/jsvi.1995.0139.

[9] Kaya, M. O. (2006). Free vibration analysis of a rotating Timoshenko beam by differential transform method. *Aircraft engineering and aerospace Technology. http://dx.doi.org/10.1108/17488840610663657.*

[10] Luintel, M. C., & Vyas, N. S. (2019). Dynamic response and stability of a spinning turbine blade subjected to pitching and yawing. *International Journal of Dynamics and Control*, 7(4), 1252-1277.http://dx.doi.org/10.13140/RG.2.2.13879.16803

[11] Hoskoti, L., Misra, A., & Sucheendran, M. M. (2021). Modal analysis of a rotating twisted and tapered Rayleigh beam. *Archive of Applied Mechanics*, 91(6), 2535-2567. https://link.springer.com/article/10.1007/s00419-021-01902-8.

[12] Rao, S. S. (2019). *Vibration of continuous systems*. John Wiley & Sons.

[13] Chung, J., & Yoo, H. H. (2002). Dynamic analysis of a rotating cantilever beam by using the finite element method. *Journal of Sound and vibration*, 249(1), 147-164. https://doi.org/10.1006/jsvi.2001.3856.

[14] Zhou, Y., Zhang, Y., & Yao, G. (2021). Nonlinear forced vibration analysis of a rotating three-dimensional tapered cantilever beam. *Journal of Vibration and Control*, 27(15-16), 1879-1892.https://doi.org/10.1177/1077546320949716